ACS Catalysis

Research Article

pubs.acs.org/acscatalysis

Photochemical Formic Acid Dehydrogenation by Iridium Complexes: Understanding Mechanism and Overcoming Deactivation

Seth M. Barrett,[‡] Samuel A. Slattery,[‡] and Alexander J. M. Miller*

Department of Chemistry, University of North Carolina at Chapel Hill, Chapel Hill, North Carolina 27599-3290, United States

Supporting Information

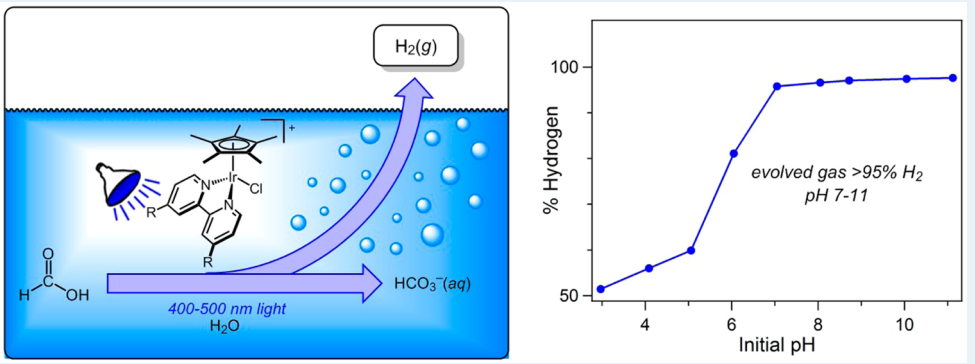

ABSTRACT: The mechanism of photochemical formic acid dehydrogenation catalyzed by $[Cp^*Ir(bpy)(Cl)]^+$ (**1**, bpy = 2,2′-bipyridine) and $[Cp^*Ir(bpy\text{-}OMe)(Cl)]^+$ (**1-OMe**, bpy-OMe = 4,4′-dimethoxy-2,2′-bipyridine) is examined. The catalysts operate with good turnover frequency (TOF) across an unusually wide pH range. Above pH 7, the evolved gas is >95% pure H_2 (along with traces of CO_2 but no detectable CO). Light-triggered H_2 release from a metal hydride intermediate is found to be the turnover-limiting step, based on the observed first-order dependence on catalyst concentration, saturation behavior in formate concentration, and direct in situ observation of a metal hydride resting state during turnover. Deactivation pathways are identified, including ligand loss and aggregate formation, precipitation of insoluble forms of the catalyst, and deprotonation of the iridium hydride intermediate. Guided by mechanistic insights, improved catalytic activity (initial TOF exceeding 50 h^{-1}), stability (>500 turnovers at nearly 5 atm), and selectivity (>95% H_2 gas) are achieved.

KEYWORDS: *hydrogen evolution, iridium, hydride, photocatalysis, hydrogen storage*

INTRODUCTION

Carbon dioxide is a promising hydrogen storage medium, capable of storing 4.3 wt % H_2 in formic acid (HCO_2H) and up to 12 wt % H_2 in subsequent hydrogenation products CH_3OH and H_2O.[1−5] The CO_2/HCO_2H couple (eq 1) is particularly promising because the process is readily reversible, as evidenced by a substantial body of work on both the CO_2 hydrogenation[6−9] and the formic acid dehydrogenation steps.[2,5,10−12]

$$H_2 + CO_2 \leftrightarrows HCO_2H \quad (1)$$

A few catalysts can perform both CO_2 hydrogenation and HCO_2H dehydrogenation.[13−17] Reversible storage and release is most commonly accomplished by applying high H_2/CO_2 pressures to promote hydrogenation, then releasing the pressure to trigger dehydrogenation.[13−16] Solution pH can also be used to control the reaction, with hydrogenation occurring at basic pH (where production of formate is thermodynamically favorable) and dehydrogenation occurring at acidic pH (where the thermochemistry shifts to favor H_2/CO_2 release).[17]

An alternative strategy for reversible hydrogen storage would utilize visible light to regulate the chemistry of eq 1. Storage would be accomplished by thermal hydrogenation of CO_2 in the dark, followed by light-triggered hydrogen release. In pursuit of this eventual goal, and motivated by our interest in photochemical H_2 evolution,[18,19] we considered the very rare examples of *photocatalytic* formic acid dehydrogenation. Building on two prior studies,[20,21] Beller and co-workers recently reported iron carbonyl catalysts that produced up to 126 turnovers of H_2:CO_2 (1:1 mixture) from formic acid in DMF solvent at 60 °C under photolysis.[22,23] In one of the only other examples of this reaction, Ziessel and co-workers demonstrated that Cp*Ir-based complexes produce H_2:CO_2 (1:1 mixture) from aqueous formate at pH 5, with a turnover number (TON) up to 53 after 2 h of irradiation under vacuum.[24] Under these acidic conditions (and in organic solvents), H_2 and CO_2 gas are coevolved in a 1:1 ratio.

Little is known about the mechanism of photochemical formic acid dehydrogenation. For example, metal carbonyl-catalyzed reactions may be initiated by photochemical CO dissociation, or photochemical H_2 release may occur, or light

Received: September 8, 2015

DOI: 10.1021/acscatal.5b01995
ACS Catal. 2015, 5, 6320−6327

could play multiple roles simultaneously.[25] Mechanistic information on the Cp*Ir-based photocatalysis is limited to an Arrhenius analysis,[24] which gave activation energies higher than the Cp*Ir-catalyzed photochemical water−gas shift reaction.[26] Photochemical formic acid dehydrogenation catalysts are currently slower and less stable than corresponding thermal catalysts.[3,27,28] A deeper mechanistic understanding of photochemical formic acid dehydrogenation would provide guidance for improving these systems, which offer a promising, mild photochemical alternative to thermal reactions controlled by pressure or pH.

The mechanistic studies reported here reveal several new aspects of Cp*Ir-photocatalyzed formic acid dehydrogenation that helped guide significant improvements in stability, activity, and selectivity. Kinetic studies and in situ reaction monitoring indicate turnover-limiting photochemical H_2 release under most conditions, directing subsequent improvements by tuning the light source wavelength and intensity. Several deactivation pathways are also identified, guiding changes to the catalyst structure and reaction conditions that yielded more active and longer-lived catalysts. The catalysts operate efficiently in basic conditions, where the evolved gas is comprised of >95% H_2 because of efficient sequestration of CO_2 by hydroxide. Our mechanistic findings lead to substantial improvements in performance, indicating that photochemical H_2 release is a promising strategy complementary to thermal reactions.

RESULTS AND DISCUSSION

Initial Catalytic Studies. The air-stable and water-soluble precatalysts **1** and **1-OMe** were prepared according to previously reported procedures.[29,30] Initial catalytic runs were carried out in 20 mL scintillation vials containing 0.36 mM precatalyst in 10 mL of 1 M aqueous sodium formate, illuminated by a 460 nm LED lamp at room temperature (Scheme 1). The evolved gas was collected in an inverted buret

Scheme 1. Typical Conditions for Photochemical Formic Acid Dehydrogenation by 1 and 1-OMe

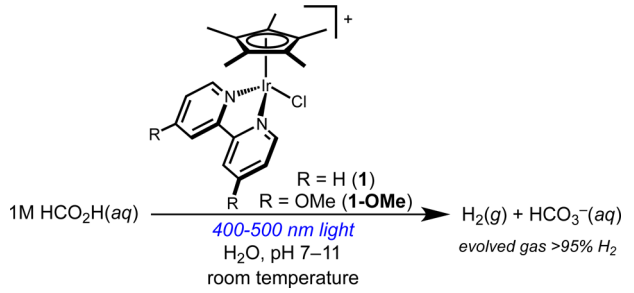

eudiometer and analyzed by headspace gas chromatography (GC) in many cases (see Experimental Section and Supporting Information for full experimental details).

When protected from light, solutions of **1** do not evolve appreciable amounts of gas at room temperature. Under 460 nm illumination, however, a pH 5 formate solution containing **1** produced 1.2 mL of gas in 2 h, corresponding to a turnover frequency (TOF) of ~4 h^{-1} (slightly higher than Ziessel's prior report, TOF = 0.5 h^{-1}).[24] Although the prior report examined only pH 5 conditions, we found that the catalyst is also active in basic solutions: upon photolysis of a pH 10 formate solution of **1**, gas evolution commenced immediately and continued steadily. The methoxy-substituted catalyst **1-OMe**, which had not been studied previously as a photocatalyst for formic acid dehydrogenation, shows significantly improved photocatalytic activity relative to **1** (Figure 1). As shown in Figure 1,

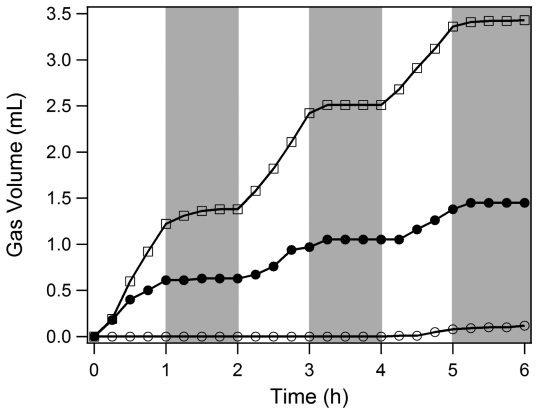

Figure 1. Gas evolution from formate solutions of **1** (●), **1-OMe** (□), and no catalyst (○) during intermittent illumination (white background: lamp on, gray background: lamp off). Conditions: 0.32 mM Ir, pH 10 1 M $NaCO_2H$(aq), 18 mM phosphate, 296 K.

intermittent illumination (1 h cycles) confirmed the critical role of visible light in promoting the reaction. In the absence of the catalyst, only traces of gas evolved over 6 h, with no response to light.

Both catalysts exhibit gradually diminishing activity during prolonged illumination. While the initial yellow color of the solutions was maintained for the first 24 h, prolonged photolysis (beyond 48 h) in the eudiometer setup led to formation of a dark, *catalytically inactive* precipitate. The chloride complexes **1** and **1-OMe** are both air-stable; however, a ~30% drop in activity was observed when the reactions were carried out under air. In order to avoid this decomposition and better understand the system, a series of mechanistic studies were carried out.

pH Dependence. The pH dependence of the photochemical reaction was examined first. The volume of evolved gas dropped noticeably at higher pH, as shown in Figures S9 and S10. Rather than indicating a loss of activity, GC headspace analysis revealed that the decline in evolved gas correlated with a decrease in the amount of CO_2 released during the reaction. In fact, H_2 comprised 96(3)% of the evolved gas above pH 7, as shown in Figure 2a (the fuel cell poison CO was not detected). After prolonged illumination, reaction mixtures with initial pH between 6 and 10 were observed to approach a final pH of 8, while more acidic solutions showed no significant pH change during the reaction. This behavior is consistent with CO_2 sequestration and engagement of carbonate equilibria above pH 6, as in eq 2 (an authentic sample of ~30 mM HCO_3^- in 1 M formate gave a pH 8 solution).

$$HCO_2^- + H_2O \leftrightarrows H_2 + HCO_3^- \quad (2)$$

When the volume of evolved gas is corrected based on the H_2:CO_2 ratio of the evolved gas, it becomes clear that the rate of H_2 evolution is faster under more basic conditions (Figure 2b). Little H_2 release activity is observed below pH 3, but the rate increases sharply between pH 3 and 5 for both **1** and **1-OMe**. Both catalysts exhibit a roughly constant TOF between pH 5 and 10, with **1-OMe** operating roughly 3 times faster than **1** over this wide pH range. Catalyst **1** maintains good

DOI: 10.1021/acscatal.5b01995
ACS Catal. 2015, 5, 6320−6327

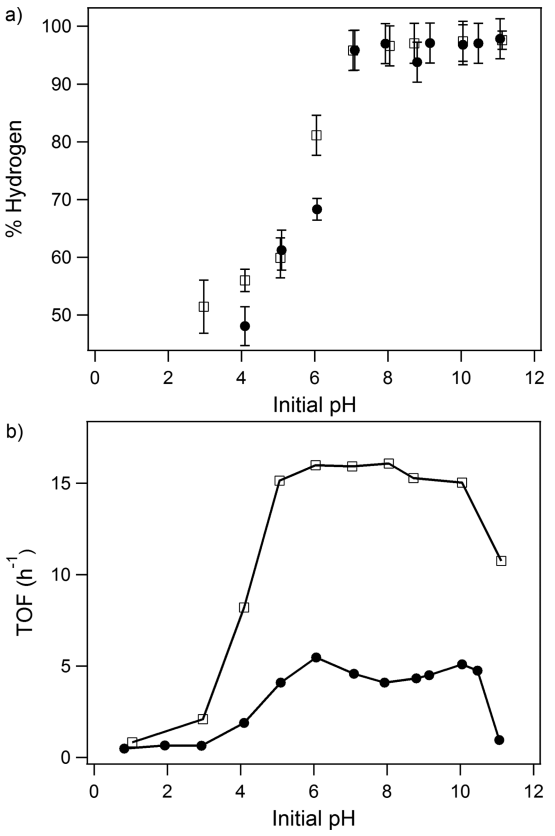

Figure 2. (a) H_2 content of evolved gas as a function of pH for **1** (●) and **1-OMe** (□). (b) Initial TOF (H_2 over 2 h) as a function of initial pH for **1** (●) and **1-OMe** (□). Conditions: 0.36 mM catalyst, 1 M $NaCO_2H$(aq), 296 K.

photocatalytic activity up to pH 10, and **1-OMe** performs well even at pH 11.

The broad region of pH independence is quite uncommon for aqueous formic acid dehydrogenation catalysts. Thermal aqueous formic acid dehydrogenation catalysts typically exhibit a sharp maximum between pH 3 and 4, close to the pK_a of formic acid (3.75).[17,31−33] The ability of the photocatalysts **1** and **1-OMe** to maintain activity under alkaline conditions enables the exciting observation of pure H_2 release. Only a few catalysts are capable of releasing a pure stream of H_2 from formic acid,[1,3,13,14,34] and this is the first example of photochemically driven production of pure H_2.

The unusual ability to release H_2 from alkaline solutions is ascribed to the intermediate $[Cp^*Ir(bpy)(H)]^+$, a species that becomes a stronger net hydride donor upon illumination.[18,19] Given that most catalysts produce 1:1 H_2:CO_2 mixtures in the "hydrogen release" step, photochemical methods offer a complementary selectivity for high-purity hydrogen gas. Basic conditions also may facilitate integration with hydrogen storage reactions, because the best CO_2 and HCO_3^- hydrogenation catalysts thrive with added base,[17,35] similar to the conditions in which our catalysts are most active.

Pressure Dependence. The dehydrogenation was carried out in a closed system to determine if H_2 inhibited the reaction. A thick-walled Pyrex glass pressure vessel was charged with a standard catalyst solution of **1-OMe** (20 mL in a ∼ 40 mL vessel), equipped with either a 4.1 or 10.9 atm pressure gauge, and sealed under N_2. Hydrogen evolved with a TOF of 10 h^{-1} under 460 nm illumination at pH 9. When a higher-powered 443 nm LED lamp was applied instead, a higher initial TOF (20 h^{-1}) was obtained and the pressure in the vessel approached 4 atm. The initial rates in the pressure vessel were similar to initial rates observed by eudiometry (which maintains 1 atm H_2 during the reaction), and pressures over 4 atm were required before H_2 pressure appeared to inhibit the reaction. This pressure range is similar to a recently reported charge−discharge process for hydrogen storage.[13]

Kinetic Analysis and in Situ Monitoring. Initial rates methods (linear fits of first 2 h of reaction) were used to determine the molecularity of the reaction. The rate of gas evolution exhibits a first-order dependence on the concentration of both catalysts **1** (Figure S11) and **1-OMe** (Figure 3a). The reaction catalyzed by **1** exhibits saturation kinetics as a

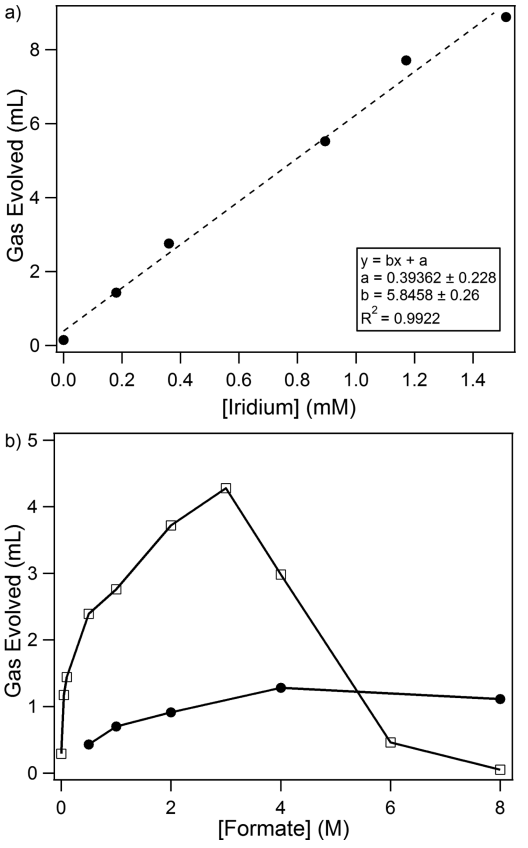

Figure 3. (a) Gas volume measured from the eudiometer after 2 h of irradiation with varying concentrations of precatalyst **1-OMe** in pH 9 1 M formate. (b) Gas evolved after 2 h of 460 nm irradiation of 0.36 mM **1** (●) and 0.36 mM **1-OMe** (□) with varying concentrations of formate at pH 9.

function of formate concentration, with the initial rate increasing at higher formate concentration before becoming formate-independent above 4 M (Figure 3b).

In contrast, an unexpected deactivation process was encountered in **1-OMe**-catalyzed reactions carried out at high formate concentrations (pH 9). As shown in Figure 3b, the rate increases initially with increasing formate concentration, but slows and eventually *loses activity* at formate concentrations around 6 M. The appearance of a yellow precipitate above 3 M formate correlates with the decrease in activity of **1-OMe**; further investigations of this deactivation process are described below.

DOI: 10.1021/acscatal.5b01995
ACS Catal. 2015, 5, 6320−6327

The pale yellow charge-transfer band of the chloride complex **1-OMe** (λ_{max} = 330 nm) provided a convenient handle for in situ ultraviolet−visible (UV−vis) spectroscopy studies. Initial studies were carried out protected from light to prevent turnover. The reaction was monitored over time immediately following injection of a stock solution of catalyst **1-OMe** to a cuvette containing a stirred solution of 1 M formate (pH 9). The characteristic charge-transfer band of the hydride complex $[Cp^*Ir(bpy\text{-}OMe)(H)]^+$ (**2-OMe**, λ_{max} = 390 nm)[18] grew in over ∼2 min (Figure 4). The hydride complex is a proposed

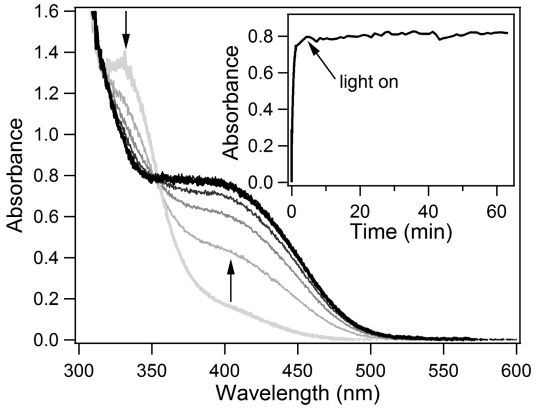

Figure 4. Absorbance profile after injection of 0.36 mM **1-OMe** into pH 9 1 M $NaCO_2H$(aq) at 296 K. The growth of **2-OMe** was observed in 20 s intervals for 1 min in the dark, followed by illumination. The inset follows the hydride absorbance at 390 nm; after 1 min in the dark, illumination with 460 nm light continued for 60 min.

intermediate in thermal formic acid dehydrogenation by Cp*Ir-based catalysts.[31,36,37] Formation of hydride **2-OMe** occurs much faster than the observed rate of catalysis, suggesting that these dark processes are not rate-limiting.

Photocatalytic dehydrogenation was then spectroscopically monitored under continuous illumination to elucidate the resting state during catalysis. The cuvette was attached to a eudiometer to confirm that H_2 was indeed released during monitoring. The charge-transfer band at 390 nm remained prominent during active catalysis (Figure 4), identifying hydride **2-OMe** as the resting state and indicating turnover-limiting photochemical H_2 release.

A significant kinetic isotope effect (KIE) is anticipated if H_2 evolution is indeed the turnover-limiting process. The initial rate of gas evolution from HCO_2H/H_2O and DCO_2D/D_2O was determined in two separate experiments, providing a normal, primary KIE of 2.6(3), as shown in Table 1. This KIE is similar to the value of 2.6(1) reported for thermal formic acid dehydrogenation by $[Cp^*Ir(4,4\text{-dihydroxy-bipyridine})(OH_2)]^{2+}$, which was also proposed to involve rate-determining H_2 evolution.[37−39]

Table 1. Kinetic Isotope Effects of Photochemical Dehydrogenation[a]

formic acid isotopologue	solvent	kinetic isotope effect
HCO_2H	H_2O	–
DCO_2D	D_2O	2.6(3)
HCO_2H	D_2O	2.4
DCO_2D	H_2O	1.8

[a]Conditions: 0.36 mM **1-OMe**, 1 M formate, pH 8, 460 nm illumination for 2 h at 296 K. The formic acid OH proton is assumed to exchange with water protons.

Table 1 shows KIE values obtained when other mixtures of isotopologues were examined. The observation that HCO_2H/D_2O mixtures produced a normal, primary KIE of similar magnitude to the DCO_2D/D_2O is inconsistent with rate-limiting hydride formation: conversion of Ir−O_2CH to Ir−H should be sensitive only to isotopic substitution on formate, and a primary KIE would be expected only when comparing rates of formate with formate-*d*. On the other hand, the KIE experiments are all consistent with a turnover-limiting process involving H−H bond formation.

Lamp Intensity, Wavelength Dependence, and Quantum Yields. A rate-limiting photochemical process could be limited by the kinetics of the photochemical reaction or by the light-absorbing characteristics. To further probe this important step, the influence of light intensity was examined. A 443 nm LED lamp with programmable output intensity was used to perform formic acid dehydrogenation between 2 and 62 mW·cm^{-2} power density. The initial TOF increased from 3 h^{-1} at low intensity to 36 h^{-1} at high intensity (Figure S20), again consistent with photochemical H_2 evolution limiting the rate of catalysis. A slight deviation from linearity was observed at high intensity, which might indicate that sufficient photon flux was present that other steps were starting to contribute to the rate.

To probe the role of overlap between the light source and the absorbing molecules, photocatalysis was performed under 406, 443, and 503 nm illumination at a constant, relatively low power density (∼13 mW·cm^{-2}) in a closed system (Figure S19). Illumination with either the 406 or 443 nm lamp gave similar activity (10 h^{-1} for **1-OMe**). Under 503 nm light, the rate dropped to 5 h^{-1} for **1-OMe**. The chloride complex **1-OMe** does not absorb as much low-energy light, nor with as much intensity as **2-OMe**, so the ability to operate with >400 nm light suggests that **2-OMe** is the active light absorber.[18] The performance trends correlate well with the predicted number of photons absorbed by hydride **2-OMe**; calculations suggest that **2-OMe** would absorb a similar number of 406 and 443 nm photons, but about 4 times fewer 503 nm photons (see derivation in Supporting Information).

The conventional TON and TOF metrics of catalysis provide a convenient point of comparison with thermal catalysts, but photochemical reactions can also be assessed based on the photon-to-chemical efficiency. The quantum yield, defined as the moles of H_2 produced divided by the moles of photons absorbed by the catalyst, was determined under several conditions. Under typical conditions of 443 nm illumination at 13 mW·cm^{-2} intensity, Φ = 0.05 is obtained for formic acid dehydrogenation by **1-OMe**. As the 443 nm lamp intensity was increased, the quantum yield decreases slightly, with Φ = 0.03 at 62 mW·cm^{-2}. As the irradiation wavelength was changed, only slight variations in quantum yield are observed, with $\Phi_{406\ nm}$ = 0.05 and $\Phi_{503\ nm}$ = 0.10 (Table S2). With relatively high photon efficiency maintained over the course of 2 h,[24,26] and under a variety of illumination conditions, catalyst **1-OMe** has encouraging photochemical behavior.

Mechanistic Proposal. A plausible catalytic mechanism that is consistent with the preceding mechanistic studies is depicted in Scheme 2. Entry to the catalytic cycle is afforded by the chloride precatalysts **1** and **1-OMe**. Previous studies have shown that $[Cp^*Ir(bpy)(Cl)][Cl]$ undergoes facile ligand exchange in water[18] and is readily converted to the hydride

DOI: 10.1021/acscatal.5b01995
ACS Catal. 2015, 5, 6320−6327

Scheme 2. Proposed Mechanism of Photochemical Formic Acid Dehydrogenation

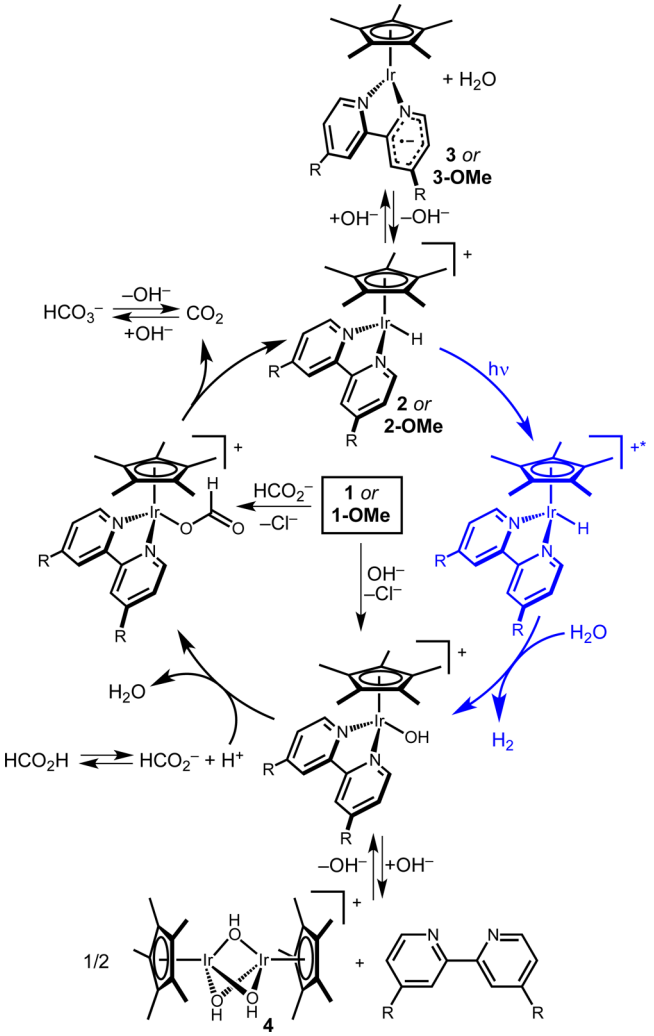

$[Cp^*Ir(bpy)(H)]^+$ in aqueous formate.[40] Ligand substitution processes are not turnover-limiting, as evidenced by the similar rates of dehydrogenation by chloride **1** and aquo $[Cp^*Ir(bpy)(H_2O)]^{2+}$ (TOF ~ 4 h^{-1} for each catalyst). Under basic conditions hydroxide substitution would be expected, based upon the reported pK_a value for aquo $[Cp^*Ir(bpy)(H_2O)]^{2+}$.[29,41,42] Indeed, stirring either chloride **1** or aquo $[Cp^*Ir(bpy)(H_2O)]^{2+}$ in a pH 10 solution leads to the formation of the same product by NMR spectroscopy, assigned as the hydroxide complex $[Cp^*Ir(bpy)(OH)]^+$. Our in situ observations of rapid conversion of chloride **1-OMe** to hydride **2-OMe** in formate solutions in the dark suggest that formate binding and decarboxylation occur rapidly and without photochemical assistance.

Photochemical H_2 release (shown in blue in Scheme 2) has been identified as the turnover-limiting process at high concentrations of formate. The first-order dependence on Ir and saturation behavior with respect to formate concentration suggest that at lower formate concentrations a pre-equilibrium step involving formate (such as reversible formation of the formate complex) is also involved in the rate law. Observation of the hydride **2-OMe** as the resting state during photocatalysis strengthens this conclusion. Finding the reaction to be photon-limited holds promise for future catalyst development: improved reaction rates are possible by supplying a higher photon flux (see above), which can be accomplished by changing the photochemical reactor design or by employing more powerful lamps.[43−45]

The precise mechanism of photochemical H_2 release warrants further discussion.[46,47] The primary event is likely excitation to the previously observed triplet excited state of **2**.[26,48,49] Once formed, the triplet excited state has a potent thermodynamic driving force for hydride transfer: the excited state is at least 20 kcal·mol^{-1} *more hydridic* than the ground state in acetonitrile.[19] While the kinetic details of excited-state H_2 release from **2** remain the subject of ongoing studies in our laboratory, the photohydride reactivity of **2** clearly enables some of the unique features of Cp*Ir-based photochemical formic acid dehydrogenation. Light absorption renders the M−H fragment more hydridic, and therefore more reactive toward weak acids (H_2O in this case), facilitating H_2 release under strongly basic conditions. Photoelectrochemical H_2 evolution proceeds efficiently until pH 10,[18] in contrast to the acidic conditions (pH ~ 4) required by most aqueous formic acid dehydrogenation catalysts. Photochemically enabling H_2 release above pH 7 in turn facilitates the release of pure H_2 gas with concomitant trapping of CO_2 by hydroxide. The rarity of pure H_2 release likely stems from the fact that basic conditions are at odds with the fundamental organometallic chemistry underlying H_2 release: the metal hydride intermediates typically require acidic conditions to rapidly release H_2.

Typical thermal H_2 release pathways slow rapidly as the solution pH increases, as indicated by the narrow, acidic pH range at which most aqueous catalysts operate.[17,31,32] In contrast, catalysts **1** and **1-OMe** operate with similar TOF over a wide pH range. Although pH does not greatly impact the reaction rate, it does impose several restrictions based on the pK_a values of various species. The pK_a of formic acid (3.75) dictates the availability of formate anion and therefore the efficiency of the substitution process; under more acidic conditions formic acid is present and undergoes substitution more slowly, as observed in related systems that exhibit maximal performance near pH 4.[31,32] The pK_a of the metal hydride limits the operational pH range in the basic regime. A pK_a of ~10 is estimated for hydride **2**, based on changes in electrochemical behavior,[18] at which point deprotonation forms an off-cycle Ir(II)-$bpy^{\bullet-}$ complex (**3**, Scheme 2).[49] When hydride **1** was stirred at pH 13, a purple precipitate formed; extraction into benzene confirmed that the precipitate was the deprotonation product **3**.[49]

Deactivation Pathways. Understanding deactivation and/or decomposition processes of homogeneous catalysts can help identify molecular weaknesses and guide catalyst redesign.[50,51] After 72 h illumination of **1** in pH 8 or pH 10 formate solutions while collecting gases by eudiometry, formation of a dark blue solution was observed. A UV−vis spectrum after the reaction revealed the growth of a broad new feature with λ_{max} = 750 nm that is consistent with nanoparticle formation.[40,52] Nanoparticles could result from photochemical or thermal bpy dissociation, forming the photocatalytically inactive *tris*-hydroxide dimer **4** (Scheme 2),[41] which could go on to form insoluble aggregates or nanoparticles.

To prevent ligand loss, the reaction was run in the presence of free 2,2′-bipyridine. In parallel eudiometry experiments monitoring the ability of **1** to dehydrogenate 1 M formate solutions at pH 9, the catalyst produced more H_2 in the presence of 3 equiv free ligand (Figure S22). Interestingly,

DOI: 10.1021/acscatal.5b01995
ACS Catal. 2015, 5, 6320−6327

analogous experiments in the sealed medium-pressure vessel showed little evidence of aggregation, suggesting that slow leaking of air into the eudiometer setup may also be partially responsible for nanoparticle formation. The more strongly donating methoxy-substituted bipyridine ligand in **1-OMe** may help avoid ligand loss during catalysis, as **1-OMe** maintains its initial rate for longer.

A deactivation process specific to **1-OMe** is encountered at high formate concentrations, as discussed above in the context of formate dependence from Figure 3b. To probe this process further, **1-OMe** was stirred in 8 M formate solutions protected from light. A yellow precipitate formed in the dark, ruling out photochemical degradation. When the solids were assessed by attenuated total reflection infrared (ATR-IR) spectroscopy, a prominent Ir−H stretch was observed at 2046 cm^{-1}, closely matching the previously reported stretch for the hexafluorophosphate salt.[42] The solids dissolved readily in CD_3CN, and NMR and electrospray ionization mass spectrometry (ESI-MS) analyses confirm the presence of hydride **2-OMe** as well as some $[Cp^*Ir(bpy\text{-}OMe)(O_2CH)]^+$. Taken together, the data suggest that the formate salt of **2-OMe**, $[Cp^*Ir(bpy\text{-}OMe)(H)][O_2CH]$, is less soluble than the chloride salt, leading to precipitation. The methoxy substituents apparently provide enough lipophilicity that the formate salt of **2-OMe** is substantially less water-soluble than the formate salt of **2**. It is noteworthy that activity can be restored simply by diluting the solution below 6 M formate.

Improved Catalytic Conditions. Guided by our mechanistic findings, catalytic activity was reassessed in a pressure vessel under conditions designed to minimize decomposition while maintaining optimal activity. When a 3 M aqueous formate solution at pH 8 was treated with 0.39 mM catalyst **1** at 296 K and illuminated with a 443 nm lamp, the initial TOF exceeds 12 h^{-1} and TON > 360 is achieved. Under analogous conditions with 0.37 mM **1-OMe**, the initial TOF exceeds 50 h^{-1} and TON > 500 is achieved over 30 h illumination. After 30 h, nearly 5 atm had built up in the sealed vessel. In addition to outperforming other photocatalysts that we are aware of, photocatalyst **1-OMe** also produces H_2 in 96% purity according to GC analysis.

CONCLUSIONS

Mechanistic studies of Cp*Ir-based photochemical formic acid dehydrogenation catalysts have led to a detailed understanding of the active catalyst cycle as well as decomposition and deactivation pathways. Direct spectroscopic evidence for every proposed intermediate was accumulated. Kinetic evidence identified the turnover-limiting process as photochemical H_2 release, via the photohydride $[Cp^*Ir(bpy)(H)]^+$, which is capable of producing H_2 beyond pH 10 and consequently enables the release of pure H_2 from formic acid in basic water. CO_2 is trapped in the alkaline solution, and no CO is produced, leading to headspace gas compositions of 96(3)% H_2. The H_2 levels are remarkably impervious to the makeup of the catalytic system, as H_2 levels above 90% were obtained regardless of catalyst loading and formate concentration (Figure S7). Guided by these mechanistic findings, improved visible light photocatalysis was realized at room temperature, even at elevated pressures of H_2. These findings offer a promising outlook for photochemical H_2 release as a strategy for hydrogen storage involving the CO_2/HCO_2H couple.

EXPERIMENTAL SECTION

General Considerations. Manipulations were performed under the inert nitrogen atmosphere of a Schlenk line or a glovebox. Water was thoroughly degassed by sparging with nitrogen before use. D_2O, DCO_2D, NaOD(aq), and DCl(aq) were purchased from Cambridge Isotopes Laboratories, Inc. $[Cp^*Ir(Cl)_2]_2$,[53] $[Cp^*Ir(bpy)(Cl)][Cl]$ (**1**),[29] and $[Cp^*Ir(bpy\text{-}OMe)(Cl)][Cl]$ (**1-OMe**)[30] were synthesized following established procedures. All other materials were readily commercially available and were used as received. UV−vis spectra were obtained with an Ocean Optics USB2000+ spectrometer with a DT-MINI-2GS deuterium/tungsten halogen light source controlled by OceanView software. ^1H NMR spectra were recorded on 400 or 600 MHz spectrometers at 25 °C. Chemical shifts are reported with respect to residual proteo solvent.[54] ESI-MS data was acquired on a Thermo Scientific LTQ-FT-ICR Mass Spectrometer. Infrared spectroscopy was carried out with a Bruker Alpha FT-IR equipped with an ATR module.

Visible light photolysis was carried out using either an EagleLight 460 nm (±12 nm at half-max intensity) LED lamp (500 lumens at 15 W; ∼ 2 mW·cm^{-2} in typical experimental conditions) or a ThorLabs multiwavelength LED source containing 406 ± 10 nm, 443 ± 9 nm, and 503 ± 13 nm LED lamps controlled by a ThorLabs LED driver for tunable power density. A Coherent $FieldMax_{II}$ Laser Power/Energy Meter (photodiode) was used for electronic photon flux measurements (to determine the number of incident photons on a sample). The quantum yield of the reaction was determined based on the moles of H_2 produced divided by the moles of *absorbed* photons after 2 h of irradiation. Measurements of pH were obtained with either a Fisher AccupHast pH probe, a Hanna pH probe, or a Hach ISFET pH probe.

Photocatalytic Formic Acid Dehydrogenation Procedures. *General Procedure A: Eudiometry.* Reactions were carried out in 20 mL scintillation vials containing a stir bar, 10 mL of pH-adjusted aqueous formate, and the desired precatalyst $[Cp^*Ir(bpy)(Cl)][Cl]$ (**1**) or $[Cp^*Ir(bpy\text{-}OMe)(Cl)][Cl]$ (**1-OMe**). Formate solutions were made by dissolving the appropriate amount of $NaCO_2H$ in HPLC grade water; pH adjustments were made by addition of dilute HCl(aq) and/or KOH(aq). In a typical reaction, an aqueous precatalyst solution containing 3.6 μmol **1** or **1-OMe** was delivered to a scintillation vial containing 10 mL of pH-adjusted formate via micropipette. Specialized vial caps were constructed using septum caps, PTFE tubing, needles, parafilm, and grease (Figure S1). Caps were sealed on each vial with grease and parafilm for an airtight seal. Once capped and sealed, the reaction vial was wrapped in aluminum foil to shield the reaction from light. A large recrystallization dish was then filled halfway with water, and a graduated centrifuge tube, filled with water, was inverted in the water of the recrystallization dish. The PTFE tubing attached to the reaction vial was placed into the inverted centrifuge tube, completing the eudiometer setup (Figure S1). All reaction vials were then degassed with N_2 from a Schlenk line by inserting a needle through the septum cap to the bottom of the solution. After degassing for at least 15 min, the eudiometer tube was once again filled with water and any trace N_2 gas left in the eudiometer (typically <0.1 mL) was recorded and subtracted from subsequent data. After the aluminum foil was removed, the samples were illuminated with

DOI: 10.1021/acscatal.5b01995
ACS Catal. 2015, 5, 6320−6327

a 460 ± 12 nm LED lamp with constant stirring from a magnetic stir bar. The gas evolved from these reactions was collected, via the PTFE tubing, in the inverted-buret style eudiometer suspended in water, and the volume of evolved gas was recorded for the duration of the experiment.

A representative photocatalytic dehydrogenation procedure, following General Procedure A, is included for completeness. In a beaker, 1.701 g (0.025 mol) of $NaCO_2H$ was dissolved in HPLC grade water; a volumetric flask was used to dilute the total solution volume to 25 mL, resulting in a 1.0 M formate solution. This solution was transferred to a beaker equipped with a stir bar. The pH was adjusted by addition of small volumes of KOH(aq). A 20 mL scintillation vial was then filled with 10 mL of the pH-adjusted solution using a micropipette. A second scintillation vial was prepared the same way, and stir bars were added to both vials. A 76.9 μL aliquot of a 0.042 M stock solution of **1-OMe** (3.25 μmol) was added to the first vial with a micropipette. The second vial was used as a control and contained no precatalyst. The specialized caps were then put on the two vials, and the vials were sealed with grease and parafilm around the cap−vial junction. Aluminum foil was wrapped around each vial to shield from light. A long needle connected to a Schlenk line was then inserted into the solution through the septum cap. The PTFE tubing was immersed into the inverted centrifuge vial. N_2 was then bubbled through the solution from the Schlenk line for at least 15 min. The inverted centrifuge vial was then refilled with water, while the end of the PTFE tubing was kept submerged. The tubing was then reinserted in the centrifuge vial. Under constant stirring, the aluminum foil was removed from the vials and the 460 nm LED lamp was turned on. Volume measurements were made periodically by inspection of the water level in the inverted centrifuge vial and recording the volume of collected gas.

General Procedure B: Pressure Vessel. Reactions were performed in ∼40 mL Pyrex glass pressure vessels equipped with a stir bar and capped with a pressure gauge (60 or 160 psig). Each vessel was charged with 20 mL of 1 M formate at pH 8−9, prepared according to the general procedure above. In a typical experiment, 100 mL of 1 M formate was prepared, transferred to a small bomb, and degassed for 20−30 min prior to being pumped into an N_2-filled glovebox. Next, 4.5−5.2 mg (7.32−8.46 μmol) **1-OMe** was weighed into a vial, and a micropipette was used to deliver 20 mL of the 1 M formate solution to the vial. The dissolved catalyst was then added to the pressure vessel along with a stir bar. The vessel was then capped with the pressure gauge to create an air-free, closed system. The vessel was then removed from the glovebox and placed in a photolysis hood. Under constant stirring, the vessel was monitored in the dark for ∼10 min prior to irradiation. After 10 min in the dark (allowing for equilibration in any temperature change between the glovebox and photolysis hood), the vessel was irradiated with LED light. At periodic intervals, the light was turned off, the pressure gauge was checked, and the pressure buildup was recorded.

GC Analysis. H_2 quantification was performed using a Varian 450-GC with a pulsed discharge helium ionizer detector. A 1.0 mL Vici Pressure-Lok Precision Analytical gastight syringe was used to sample the headspace of the reaction vials by puncturing the septum cap. Calibration curves were constructed independently for H_2 and CO_2. Mixed gas samples for calibration were prepared by performing gas dilutions in sealed round-bottom flasks. Data for each gas mixture was collected at least three times. The instrument is considerably more sensitive to CO_2, with even small amounts leading to substantial response. The resulting calibration curves for H_2 (Figure S3) and CO_2 (Figure S4) were validated by comparison with an authentic sample of 50/50 H_2/CO_2, purchased from Airgas (certificate of analysis: 51 ± 2% H_2). The commercial 50/50 H_2/CO_2 sample was 48 ± 2% H_2 and 52 ± 4% CO_2 according to the calibration curves.

Quantification of Catalytic Activity. Turnover number (TON) is defined as the moles of H_2 produced divided by the moles of catalyst present in the reaction. Based on the H_2 composition of the evolved gas determined by GC, the moles of H_2 were calculated from the total volume of gas evolved. Turnover frequency (TOF) is calculated by dividing the TON by the time of reaction (the irradiation time). TOF values are typically calculated as initial rates, using the first 2 h of the reaction, over which time the TOF was constant. Many experiments were run three times to ensure consistency and minimize experimental error. Error bars represent the standard deviation when two or more experiments were performed. When only one experiment was performed, uncertainty of ±3% was assigned based on typical run-to-run variation and the GC instrument response variation.

■ ASSOCIATED CONTENT

Supporting Information

The Supporting Information is available free of charge on the ACS Publications website at DOI: 10.1021/acscatal.5b01995.

Additional experimental details, photographs of reaction setups, and NMR spectra (PDF)

■ AUTHOR INFORMATION

Corresponding Author

*E-mail: ajmm@email.unc.edu.

Author Contributions

‡S.M.B. and S.A.S.: These authors contributed equally.

Notes

The authors declare no competing financial interest.

■ ACKNOWLEDGMENTS

We gratefully acknowledge funding from the University of North Carolina at Chapel Hill for the University Research Council's James Moeser Award and a J. Thurman Frieze Research Fellowship (S.A.S.) and from the NSF (Graduate Research Fellowship to S.M.B.; DGE-1144081). This research made use of an IR spectrometer funded by the UNC EFRC: Center for Solar Fuels, an Energy Frontier Research Center supported by the U.S. Department of Energy, Office of Science, Office of Basic Energy Sciences, under Award DE-SC0001011.

■ REFERENCES

(1) Zaidman, B.; Wiener, H.; Sasson, Y. *Int. J. Hydrogen Energy* **1986**, *11*, 341−347.
(2) Fukuzumi, S.; Suenobu, T. *Dalton Trans.* **2013**, *42*, 18−28.
(3) Grasemann, M.; Laurenczy, G. *Energy Environ. Sci.* **2012**, *5*, 8171−8181.
(4) Enthaler, S.; von Langermann, J.; Schmidt, T. *Energy Environ. Sci.* **2010**, *3*, 1207−1217.
(5) Johnson, T. C.; Morris, D. J.; Wills, M. *Chem. Soc. Rev.* **2009**, *39*, 81−88.
(6) Appel, A. M.; Bercaw, J. E.; Bocarsly, A. B.; Dobbek, H.; DuBois, D. L.; Dupuis, M.; Ferry, J. G.; Fujita, E.; Hille, R.; Kenis, P. J. A.; Kerfeld, C. A.; Morris, R. H.; Peden, C. H. F.; Portis, A. R.; Ragsdale,

DOI: 10.1021/acscatal.5b01995
ACS Catal. 2015, 5, 6320−6327

S. W.; Rauchfuss, T. B.; Reek, J. N. H.; Seefeldt, L. C.; Thauer, R. K.; Waldrop, G. L. *Chem. Rev.* **2013**, *113*, 6621−6658.
(7) Wang, W.; Wang, S.; Ma, X.; Gong, J. *Chem. Soc. Rev.* **2011**, *40*, 3703−3727.
(8) Jessop, P. G.; Joó, F.; Tai, C.-C. *Coord. Chem. Rev.* **2004**, *248*, 2425−2442.
(9) Jessop, P. G.; Ikariya, T.; Noyori, R. *Chem. Rev.* **1995**, *95*, 259−272.
(10) Fukuzumi, S. *Eur. J. Inorg. Chem.* **2008**, *2008*, 1351−1362.
(11) Fukuzumi, S.; Yamada, Y.; Suenobu, T.; Ohkubo, K.; Kotani, H. *Energy Environ. Sci.* **2011**, *4*, 2754−2766.
(12) Fujita, E.; Muckerman, J. T.; Himeda, Y. *Biochim. Biophys. Acta, Bioenerg.* **2013**, *1827*, 1031−1038.
(13) Papp, G.; Csorba, J.; Laurenczy, G.; Joó, F. *Angew. Chem., Int. Ed.* **2011**, *50*, 10433−10435.
(14) Boddien, A.; Gärtner, F.; Federsel, C.; Sponholz, P.; Mellmann, D.; Jackstell, R.; Junge, H.; Beller, M. *Angew. Chem., Int. Ed.* **2011**, *50*, 6411−6414.
(15) Boddien, A.; Federsel, C.; Sponholz, P.; Mellmann, D.; Jackstell, R.; Junge, H.; Laurenczy, G.; Beller, M. *Energy Environ. Sci.* **2012**, *5*, 8907−8911.
(16) Hsu, S.-F.; Rommel, S.; Eversfield, P.; Muller, K.; Klemm, E.; Thiel, W. R.; Plietker, B. *Angew. Chem., Int. Ed.* **2014**, *53*, 7074−7078.
(17) Hull, J. F.; Himeda, Y.; Wang, W.-H.; Hashiguchi, B.; Periana, R.; Szalda, D. J.; Muckerman, J. T.; Fujita, E. *Nat. Chem.* **2012**, *4*, 383−388.
(18) Pitman, C. L.; Miller, A. J. M. *ACS Catal.* **2014**, *4*, 2727−2733.
(19) Barrett, S. M.; Pitman, C. L.; Walden, A. G.; Miller, A. J. M. *J. Am. Chem. Soc.* **2014**, *136*, 14718−14721.
(20) Onishi, M. *J. Mol. Catal.* **1993**, *80*, 145−149.
(21) Linn, D. E.; King, R. B.; King, A. D. *J. Mol. Catal.* **1993**, *80*, 151−163.
(22) Boddien, A.; Loges, B.; Gärtner, F.; Torborg, C.; Fumino, K.; Junge, H.; Ludwig, R.; Beller, M. *J. Am. Chem. Soc.* **2010**, *132*, 8924−8934.
(23) Loges, B.; Boddien, A.; Junge, H.; Noyes, J. R.; Baumann, W.; Beller, M. *Chem. Commun.* **2009**, *28*, 4185−4187.
(24) Watson, K. J.; Ziessel, R. *Inorg. Chim. Acta* **1992**, *197*, 125−127.
(25) Loges, B.; Boddien, A.; Junge, H.; Beller, M. *Angew. Chem., Int. Ed.* **2008**, *47*, 3962−3965.
(26) Ziessel, R. *J. Am. Chem. Soc.* **1993**, *115*, 118−127.
(27) Boddien, A.; Mellmann, D.; Gartner, F.; Jackstell, R.; Junge, H.; Dyson, P. J.; Laurenczy, G.; Ludwig, R.; Beller, M. *Science* **2011**, *333*, 1733−1736.
(28) Bielinski, E. A.; Lagaditis, P. O.; Zhang, Y.; Mercado, B. Q.; Würtele, C.; Bernskoetter, W. H.; Hazari, N.; Schneider, S. *J. Am. Chem. Soc.* **2014**, *136*, 10234−10237.
(29) Dadci, L.; Elias, H.; Frey, U.; Hoernig, A.; Koelle, U.; Merbach, A. E.; Paulus, H.; Schneider, J. S. *Inorg. Chem.* **1995**, *34*, 306−315.
(30) Himeda, Y.; Onozawa-Komatsuzaki, N.; Sugihara, H.; Kasuga, K. *Organometallics* **2007**, *26*, 702−712.
(31) Himeda, Y. *Green Chem.* **2009**, *11*, 2018−2022.
(32) Fukuzumi, S.; Kobayashi, T.; Suenobu, T. *J. Am. Chem. Soc.* **2010**, *132*, 1496−1497.
(33) Fukuzumi, S.; Kobayashi, T.; Suenobu, T. *ChemSusChem* **2008**, *1*, 827−834.
(34) Wiener, H.; Sasson, Y.; Blum, J. *J. Mol. Catal.* **1986**, *35*, 277−284.
(35) Tanaka, R.; Yamashita, M.; Nozaki, K. *J. Am. Chem. Soc.* **2009**, *131*, 14168−14169.
(36) Himeda, Y.; Onozawa-Komatsuzaki, N.; Miyazawa, S.; Sugihara, H.; Hirose, T.; Kasuga, K. *Chem. - Eur. J.* **2008**, *14*, 11076−11081.
(37) Wang, W.-H.; Xu, S.; Manaka, Y.; Suna, Y.; Kambayashi, H.; Muckerman, J. T.; Fujita, E.; Himeda, Y. *ChemSusChem* **2014**, *7*, 1976−1983.
(38) Wang, W.-H.; Hull, J. F.; Muckerman, J. T.; Fujita, E.; Hirose, T.; Himeda, Y. *Chem. - Eur. J.* **2012**, *18*, 9397−9404.
(39) Wang, W.-H.; Ertem, M. Z.; Xu, S.; Onishi, N.; Manaka, Y.; Suna, Y.; Kambayashi, H.; Muckerman, J. T.; Fujita, E.; Himeda, Y. *ACS Catal.* **2015**, *5*, 5496−5504.
(40) Miller, A. J. M.; Heinekey, D. M.; Mayer, J. M.; Goldberg, K. I. *Angew. Chem., Int. Ed.* **2013**, *52*, 3981−3984.
(41) Makihara, N.; Ogo, S.; Watanabe, Y. *Organometallics* **2001**, *20*, 497−500.
(42) Ogo, S.; Kabe, R.; Hayashi, H.; Harada, R.; Fukuzumi, S. *Dalton Trans.* **2006**, 4657−4663.
(43) Garlets, Z. J.; Nguyen, J. D.; Stephenson, C. R. J. *Isr. J. Chem.* **2014**, *54*, 351−360.
(44) Andrews, R. S.; Becker, J. J.; Gagné, M. R. *Angew. Chem., Int. Ed.* **2012**, *51*, 4140−4143.
(45) Elliott, L. D.; Knowles, J. P.; Koovits, P. J.; Maskill, K. G.; Ralph, M. J.; Lejeune, G.; Edwards, L. J.; Robinson, R. I.; Clemens, I. R.; Cox, B.; Pascoe, D. D.; Koch, G.; Eberle, M.; Berry, M. B.; Booker-Milburn, K. I. *Chem. - Eur. J.* **2014**, *20*, 15226−15232.
(46) Esswein, A. J.; Nocera, D. G. *Chem. Rev.* **2007**, *107*, 4022−4047.
(47) Teets, T. S.; Nocera, D. G. *Chem. Commun.* **2011**, *47*, 9268−9274.
(48) Suenobu, T.; Guldi, D. M.; Ogo, S.; Fukuzumi, S. *Angew. Chem., Int. Ed.* **2003**, *42*, 5492−5495.
(49) Ladwig, M.; Kaim, W. *J. Organomet. Chem.* **1992**, *439*, 79−90.
(50) Widegren, J. A.; Finke, R. G. *J. Mol. Catal. A: Chem.* **2003**, *198*, 317−341.
(51) Crabtree, R. H. *Chem. Rev.* **2012**, *112*, 1536−1554.
(52) Hoertz, P. G.; Kim, Y.-I.; Youngblood, W. J.; Mallouk, T. E. *J. Phys. Chem. B* **2007**, *111*, 6845−6856.
(53) White, C.; Yates, A.; Maitlis, P. M.; Heinekey, D. M. (η5-Pentamethylcyclopentadienyl)Rhodium and -Iridium Compounds. In *Inorganic Syntheses*; Grimes, R. N., Ed.; John Wiley & Sons, Inc.: Hoboken, NJ, 1992; Vol. *29*, pp 228−234.
(54) Fulmer, G. R.; Miller, A. J. M.; Sherden, N. H.; Gottlieb, H. E.; Nudelman, A.; Stoltz, B. M.; Bercaw, J. E.; Goldberg, K. I. *Organometallics* **2010**, *29*, 2176−2179.

DOI: 10.1021/acscatal.5b01995
ACS Catal. 2015, 5, 6320−6327